Bioplastic Thickness Estimation Using Terahertz Time-Domain Spectroscopy and Machine Learning

Juan-Jesús Garrido-Arismendis[1], Luis Juarez[2], Jorge Mogollon[3], Brenda Acevedo-Juárez[4], Himer Avila-George*[5], Wilson Castro[6]
Facultad de Ingeniería de Industrias, Alimentarias y Biotecnología, Universidad Nacional de Frontera, Sullana, Perú[1,2,6]
Vicepresidencia de Investigación, Universidad Nacional de Cañete, Cañete, Perú[3]
Departamento de Ciencias Naturales y Exactas, Universidad de Guadalajara, Ameca, México[4]
Departamento de Ciencias Computacionales e Ingenierías, Universidad de Guadalajara, Ameca, México[5]

***Abstract*—In the sustainable packaging industry, multiple parameters require regulation to achieve a high-quality final product that meets contemporary demands. In bioplastic manufacturing, the control of the film thickness is critical because it influences the mechanical properties and other key characteristics. Terahertz time-domain spectroscopy (THz-TDS) has emerged as a promising technology for the non-invasive characterization of polymeric materials. The present study evaluates the integration of THz-TDS with chemometric techniques and machine learning models to predict the thickness of bioplastic samples fabricated from potato and maize starch. Three distinct thickness levels were produced by solution casting, and a spectral analysis was performed in the range of 0.5 to 1.2 THz. Four regression models were developed, including partial least squares regression, support vector regression, binary regression tree, and a feedforward neural network. The performance of the model was assessed using the coefficient of determination (R^2), root mean square error (RMSE) and the ratio of performance to deviation (RPD). R^2 values ranged from 0.8379 to 0.9757, the RMSE values ranged from 0.1259 to 0.3368, and the RPD values ranged from 2.4399 to 6.8106. These findings underscore the potential of THz-TDS and machine learning for non-invasive analysis of thin polymeric films and lay the groundwork for future research aimed at enhancing reliability and functionality.**

***Keywords*—Terahertz spectroscopy; machine learning; chemometrics; thickness; bioplastic**

I. Introduction

The preservation of the environment for future generations has become a growing necessity in contemporary society, which requires the pursuit of sustainable solutions, as highlighted by [1]. Among the most urgent environmental challenges is the widespread pollution caused by the widespread reliance on petroleum-derived plastics, which, according to [2] and [3], inflicts profound and measurable damage on ecosystems. Inadequate management of plastic waste in numerous regions exacerbates this issue, leading to significant amounts of pollutants entering marine ecosystems, where they persist for centuries [4], [5].

Simultaneously, as noted by [6], global population growth has driven an unprecedented rise in the demand for polymeric materials, further amplifying concerns regarding the environmental footprint of plastic waste. In response, circular bioeconomy strategies, described by [7], have gained traction, leveraging renewable biological resources to mitigate the negative impacts associated with conventional plastics. This shift has spurred the development of biodegradable polymeric materials as viable alternatives to petroleum-based plastics [8], [9]. The agro-industrial sectors, as demonstrated by [10], generate considerable amounts of by-products that offer promising feedstocks for the production of bioplastics. However, the commercialization of bioplastics still faces technical barriers, including insufficient mechanical and barrier properties as well as elevated hydrophilicity [11], [12].

Various analytical techniques have been employed to characterize biopolymeric materials. Invasive methods such as X-ray fluorescence, energy dispersive spectroscopy, and thermogravimetric analysis have been used to assess structural composition and biodegradability [13], while non-invasive approaches such as Fourier transform infrared spectroscopy, X-ray diffraction, and scanning electron microscopy have contributed to understanding material properties [14], [15]. More recently, terahertz time-domain spectroscopy (THz-TDS) has emerged as a promising tool for evaluating the crystallinity and structural characteristics of complex starch and fatty acid composites [16].

Among the physical parameters that determine bioplastic quality, film thickness is of paramount importance, as described by [17] and [18]. Thickness plays a crucial role in modulating key properties such as elongation, water vapor transmission rates, tensile strength, and light-blocking capacity [19], [20]. Furthermore, as noted by [21] and [22], thickness influences degradation rates, where a lower surface-to-volume ratio may accelerate biodegradation, and also serves as an indicator of load-bearing capacity and the onset of embrittlement. Control over thickness during fabrication is closely related to the volume of plasticizers and suspended solids used, as well as the quantity of material introduced into the molds [23], [24].

Terahertz time-domain spectroscopy operates within the frequency range of 0.1 to 10 THz, bridging the spectral gap between microwaves and far-infrared radiation, and offering simultaneous insights into both the internal structure and chemical composition of the samples, as described by [25] and [26]. In addition, the integration of chemometric techniques, which leverage mathematical and statistical tools to improve the interpretability of complex spectral data, significantly improves the robustness and reliability of analytical results, as reported by [27].

In this context, THz-TDS has gained attention as a non-invasive tool for characterizing polymeric materials, but its

combination with machine learning for bioplastic analysis is still underdeveloped. In this study, we introduce a novel approach that integrates THz-TDS with four machine learning models—partial least squares regression (PLSR), support vector regression (SVR), binary regression tree (BRT), and a feedforward neural network (FFNN)—to predict the thickness of bioplastic films made from agro-industrial by-products, specifically maize and potato starch. Although previous research has explored chemometric models and THz-TDS independently, the use of FFNN in this application is, to the best of our knowledge, unprecedented. In addition, we applied a model optimization process to improve predictive accuracy and robustness. This integrated methodology offers a new pathway for advancing non-invasive quality control in the production of sustainable packaging materials.

II. Materials and Methods

This section outlines the methodology for the fabrication, analysis, and modeling of bioplastic samples derived from maize and potato starch. The procedure is organized into three subsections: sample fabrication, THz spectroscopy, and regression analysis; see Fig. 1. Each subsection details the experimental steps and provides a rationale for the chosen methods.

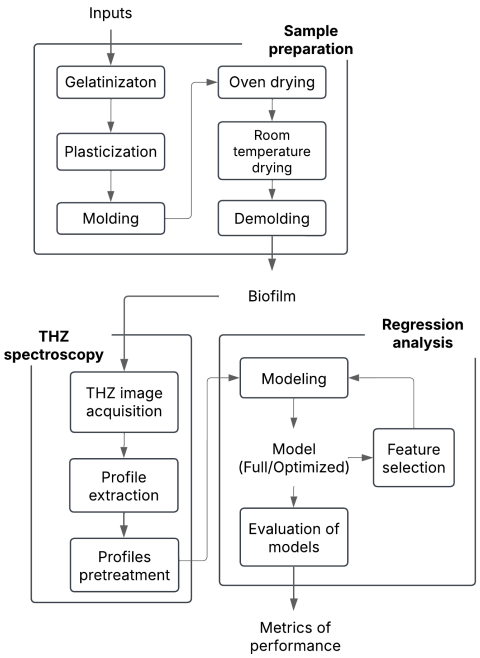

Fig. 1. Workflow of the experimental methodology for bioplastic film thickness estimation. The process includes sample fabrication from potato and maize starch, non-invasive spectral acquisition using THz-TDS, and machine learning-based regression modeling to predict film thickness.

A. Sample Preparation

Bioplastic samples were prepared using an adapted solution casting method based on established protocols [28] and [29]. Raw materials were obtained from a high-purity reagent supplier in Piura, Peru. The formulation consisted of potato starch (PS), maize starch (MS), laboratory-grade polyvinyl alcohol (PVA) (98% purity), technical-grade glycerin (97% purity), and distilled water.

The following procedure details the standardized protocol implemented to ensure uniform experimental conditions and reproducibility of results:

1) Gelatinizaton: Initially, 12 g of starch was gelatinized by dissolving it in 400 ml of distilled water at 70°C for 45 minutes with continuous stirring using a glass rod, ensuring complete dispersion, as indicated by [30].
2) Plasticization: Next, 7 ml of glycerin and 8 g of PVA (pre-diluted in 100 ml of distilled water) were added to plasticize the mixture. The mixture was stirred at 80°C for 45 minutes to enhance mechanical properties [31].
3) Molding: The plastified mixture was then poured into 9-cm-diameter Petri dishes in volumes of 12, 15, and 18 ml.
4) Oven drying: The mixture was dried in an oven at 45°C for 22 hours.
5) Room-temperature drying: An additional drying step was performed at room temperature (24°C in Sullana, Piura) within a desiccator containing blue indicator silica gel for 24 hours.
6) Demolding: Finally, the samples were removed from the Petri dishes and cut into sheets of 1.5 cm × 4.5 cm. Their thickness was determined by averaging measurements from 10 different points using a digital micrometer (range: 0 to 25 mm, resolution: 0.001 mm) [32], [33].

This fabrication process ensured uniform bioplastic films with controlled thickness, setting the stage for subsequent spectral analysis.

B. THz Spectroscopy

The fabricated samples were analyzed using a THz TeraSmart Compact Industry-Proven spectrometer (Germany), see the scheme in Fig. 2a. This device operates in transmission mode under conditions of ambient temperature and relative humidity 50%. The system had a scan range of 850 ps, a resolution of 1.2 GHz, and a spectral range of 6 THz. Each sample was placed in a polylactic acid sample holder mounted on a displacement tower; likewise, data acquisition and conversion to a MATLAB compatible format were managed using software provided by Menlo Systems.

Subsequently, spectral profiles were extracted from intensity images obtained by the spectrometer. The intensity images acquired from the spectrometer were processed in MATLAB (version R2024a, The MathWorks, Inc., USA) to distinguish the sample region from the reference (air), see Fig. 2(b). The images were segmented into nine homogeneous regions of interest (ROIs), and the average spectral pulse was extracted from each ROI, see Fig. 3(a); obtaining 162 THz pulses which were recorded in the time domain.

Finally, these spectral profiles were pre-processed by cropping to isolate the primary signal and eliminate Fabry-Perot (FP) interference (as illustrated in Fig. 3). Fig. 3(a) shows the

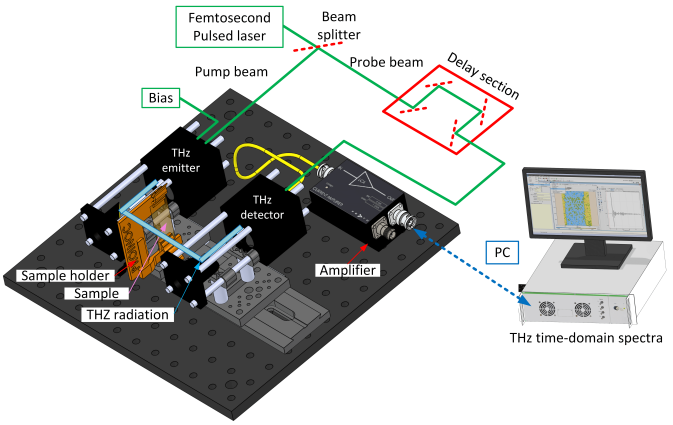

(a)

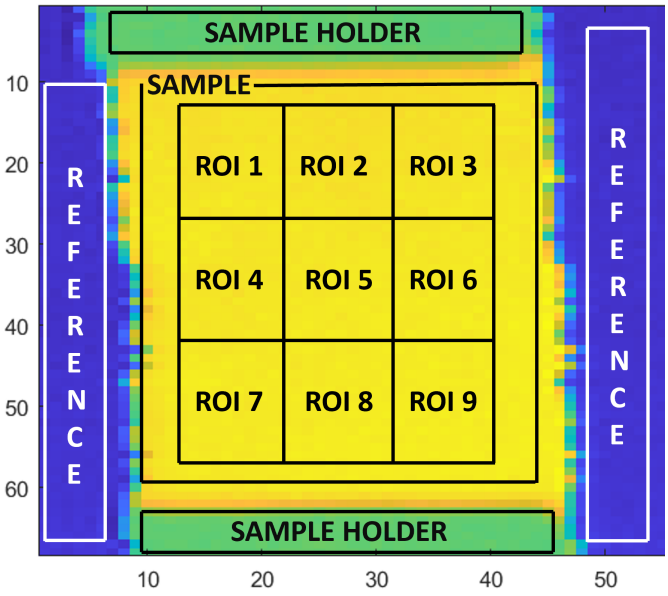

(b)

Fig. 2. Experimental setup for THz-TDS analysis of bioplastic films. (a) Schematic of the THz-TDS system operating in transmission mode under ambient conditions. (b) Representative transmittance image showing the contrast between the bioplastic sample area and the reference.

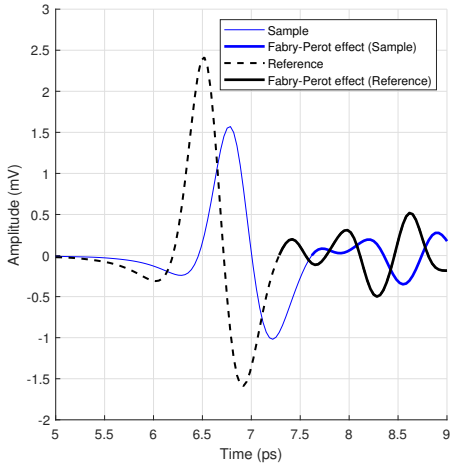

(a) Time-domain profile with FP reflections

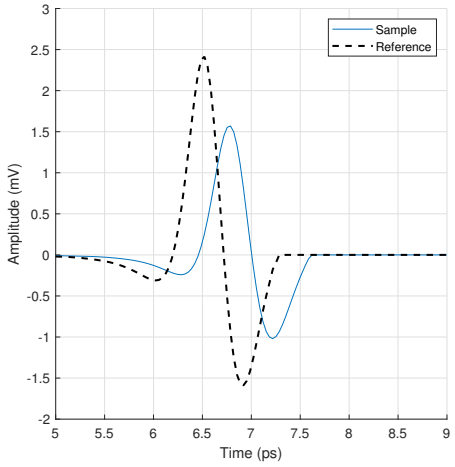

(b) Time-domain profile without FP reflections

Fig. 3. Removal of Fabry-Perot interference from THz time-domain profiles. (a) Time-domain spectra of bioplastic samples and reference, showing multiple internal reflections that distort the primary pulse, visible as secondary oscillations following the main signal peak. (b) Cropped spectra after isolating the primary pulse and removing Fabry-Perot reflections, enhancing signal clarity for subsequent frequency-domain analysis via FFT. The horizontal axis shows time in picoseconds and the vertical axis shows signal amplitude in millivolts.

complete THz spectra in the time domain within the range of 5 to 9 ps. In contrast, Fig. 3(b) illustrates the cropped spectra, capturing only the primary pulse signal and eliminating FP effects and interference. Finally, the cropped signals were transformed into the frequency domain via a fast Fourier transform (FFT) according to the Eq. 1.

$$E(\omega) = \frac{1}{\sqrt{2\pi}} \int_{-\infty}^{\infty} E(t) e^{-i\omega t}\, dt, \tag{1}$$

where $E(t)$ denotes the time-domain pulse and $E(\omega)$ its frequency-domain counterpart.

C. Regression Analysis

Four regression models were used to predict the thickness of the film from the frequency-domain data. The selected models are commented on below: include partial least squares regression (PLSR), binary regression tree (BRT), support vector regression (SVR), and a feedforward neural network (FFNN). Each model was chosen for its ability to manage the complex, multidimensional nature of the spectral data.

- Partial Least Squares Regression: This chemometric method reduces the dimensionality of the data by identifying latent variables that maximize the covariance between the predictors and the response variable [34]. PLSR was implemented using the `plsregress` function with five latent components.

- Binary Regression Tree: BRT is effective for modeling non-linear relationships and complex dependencies between variables [35]. The model was constructed using the `fitrtree` function, with a maximum of 20 node splits and a minimum of one observation per leaf, without pruning.
- Support Vector Regression: SVR adapts the principles of support vector machines for regression tasks [36]. It was implemented using the `fitrsvm` function with a radial basis function (RBF) kernel to capture intricate patterns in the data. Manual hyperparameter tuning was not performed.
- Feedforward Neural Network: This model is widely used to analyze relationships between input and output variables in non-linear datasets [37]. This artificial neural network was constructed with a hidden layer comprising 10 neurons (using a sigmoid activation function) and one output neuron with a linear activation function. The network was developed using the `feedforwardnet` function.

Optimization was carried out using the beta coefficient technique, following the approach described by [38]. Subsequently, these optimized models were applied in all regression analyzes.

Finally, to facilitate comparison of model performance metrics, a five-fold cross-validation procedure was used, repeated 30 times, to assess the generalizability of each model. The performance of the model was evaluated using the coefficient of determination (R^2), root mean square error (RMSE) and the ratio of performance to deviation (RPD). These metrics are further described in [39].

III. Results

This section presents the experimental findings, beginning with a detailed analysis of the spectral responses in the time and frequency domains. Then comes a comprehensive evaluation of the regression models developed to predict film thickness.

A. THz Spectral Analysis

1) Time-Domain Profiles: Fig. 4 illustrates the time-domain profiles, where the wave amplitudes (in microvolts) are plotted as a function of time (in picoseconds) for three distinct thickness levels of samples fabricated from potato starch, maize starch and an equal proportion mixture (EPM).

In all cases, the reference signal (air) exhibited a shorter arrival time and higher amplitude compared to the sample signals. In particular, for PS and MS samples, an increase in thickness resulted in a decrease in amplitude and a slight delay in pulse arrival. In contrast, the EPM samples did not exhibit a consistent trend. These observations suggest that the thickness of the film significantly influences the transmittance and signal timing. In summary, the time-domain analysis confirms that thickness variations lead to discernible changes in the THz pulse characteristics.

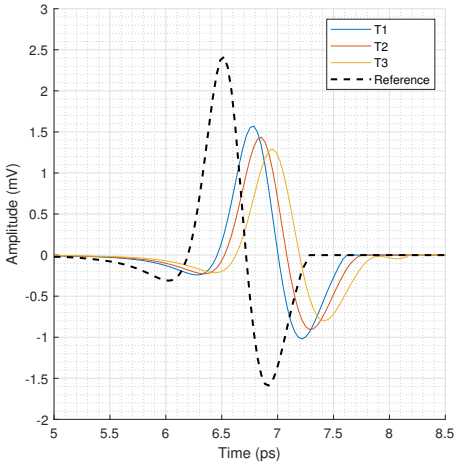

(a) PS

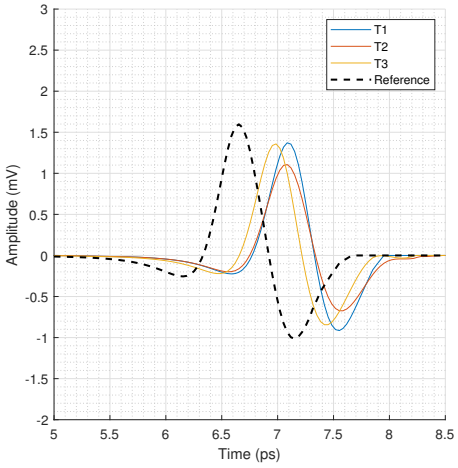

(b) EPM

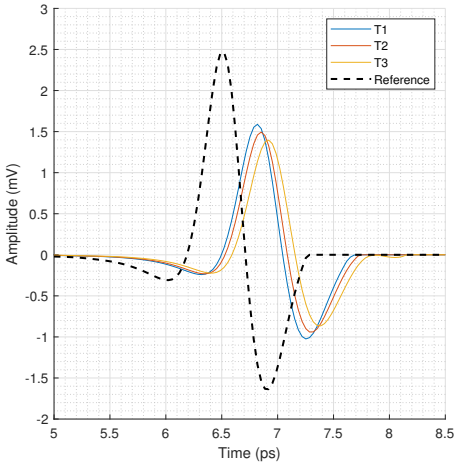

(c) MS

Fig. 4. Time-domain terahertz pulse profiles for films with three different thickness levels (T1, T2, T3) fabricated from PS, EPM, and MS.

2) Frequency-Domain Profiles: Fig. 5 displays the corresponding frequency-domain profiles obtained using FFT of the time-domain signals. A semilogarithmic scale was utilized to highlight the onset of spectral noise.

The analysis revealed that thinner samples exhibit higher signal intensity, while thicker samples demonstrate greater absorption, particularly within the 0.5 to 1.2 THz range. This range was identified as the most sensitive to thickness variations and was therefore selected for subsequent regression modeling. Additionally, noise beyond 1.4 THz was consistently observed across all measurements, likely due to ambient humidity absorption. In general, the frequency domain analysis reinforces the influence of sample thickness on spectral response and provides the basis for predictive modeling of film thickness.

B. THz Profile Modeling and Comparison of Statistical Metrics

The predictive performance of four regression models—partial least squares regression, binary regression tree, support vector regression, and a feedforward neural network—was evaluated using the frequency-domain data. Tables I and II present plots comparing the actual versus predicted thickness values for both the full and optimized versions of the models.

Table III summarizes the performance metrics for full and optimized models in each type of sample. Regarding R^2, FFNN and PLSR generally achieved the highest values. In PS samples, FFNN reached 0.9757 $\pm$ 0.0104 and 0.9625 $\pm$ 0.0157 for the full and optimized versions, respectively. In EPM, both FFNN and BRT showed a lower initial performance but improved slightly after optimization. In MS, the optimized PLSR model reached the best R^2 value of 0.9504 $\pm$ 0.0048. For RMSE, the lowest value in PS appeared in the full FFNN model (0.1259 $\pm$ 0.0263), while in EPM, the RMSE values were relatively high in all models. In MS, the optimized PLSR model showed a marked improvement from 0.2351 $\pm$ 0.0039 (full) to 0.1819 $\pm$ 0.0141 (optimized). Regarding RPD, the highest PS value was observed in the full FFNN model, while the EPM values remained between 2.4 and 2.8, indicating the need for further refinement. In MS, the optimized PLSR model increased RPD from 3.4723 $\pm$ 0.0583 (full) to 4.4899 $\pm$ 0.1326, improving robustness.

In general, higher R^2 values corresponded to lower RMSE. In PS, FFNN offered the best balance of R^2 and RMSE, while in EPM, some models achieved relatively high R^2 but retained substantial RMSE. In MS, optimized models improved predictive accuracy without sacrificing generalization capacity. Optimization had a positive effect in most cases, although EPM showed variable improvement, particularly in BRT and FFNN. PLSR in MS presented a substantial gain in R^2 and a decrease in RMSE.

Differences in performance metrics were found for different sample types. PS showed the best results, whereas EPM presented greater predictive challenges. MS offered intermediate performance, which improved considerably with optimization. The best models identified for each sample were FFNN for PS, optimized BRT and FFNN for EPM, and optimized PLSR for MS.

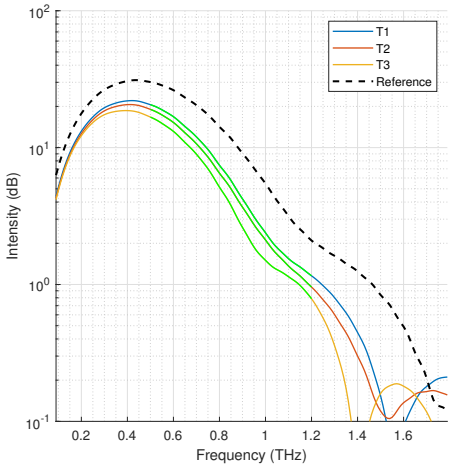

(a) PS

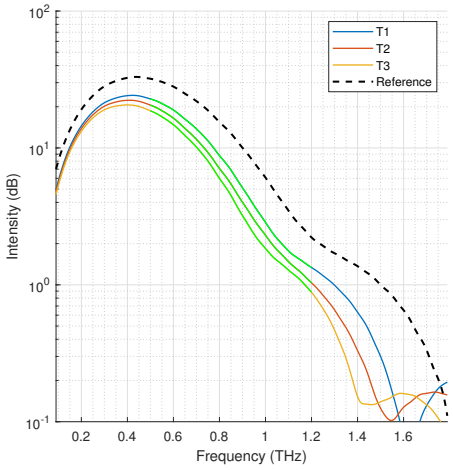

(b) EPM

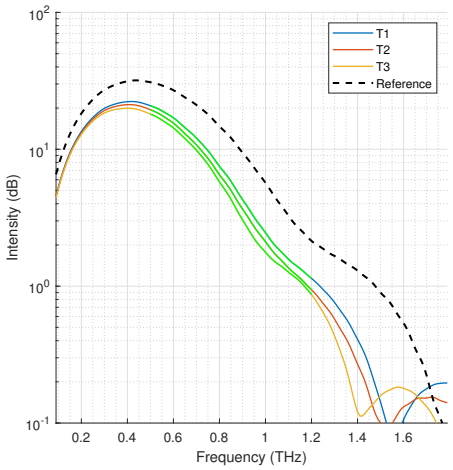

(c) MS

Fig. 5. Frequency-domain terahertz spectra of bioplastic films with three thickness levels (T1, T2, T3) fabricated from PS, EPM, and MS.

TABLE I. REAL VS. PREDICTED THICKNESS USING NON-OPTIMIZED MODELS. SCATTER PLOTS FOR SVR, BRT, PLSR, AND FFNN APPLIED TO PS, EPM, AND MS FILMS. THE 45° LINE REPRESENTS IDEAL PREDICTIONS; TREND LINES SHOW MODEL FIT

Models	PS	EPM	MS
SVR	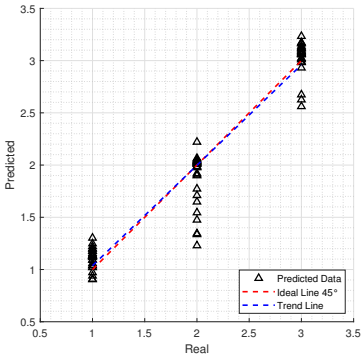	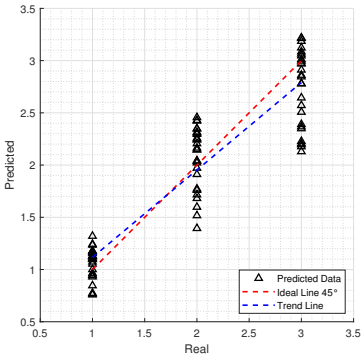	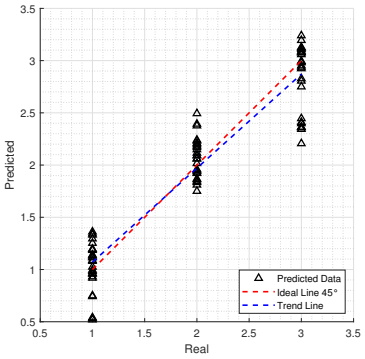
BRT	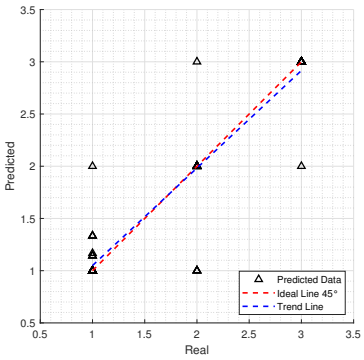	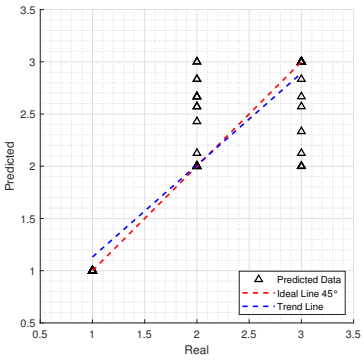	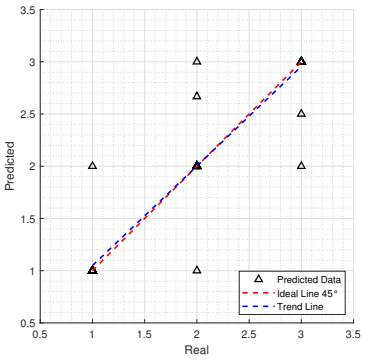
PLSR	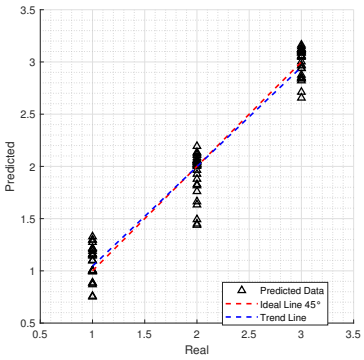	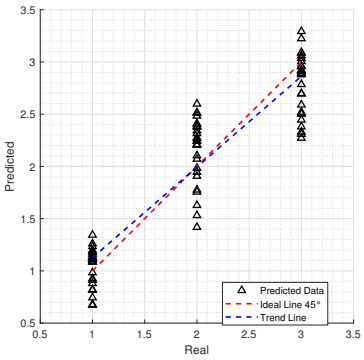	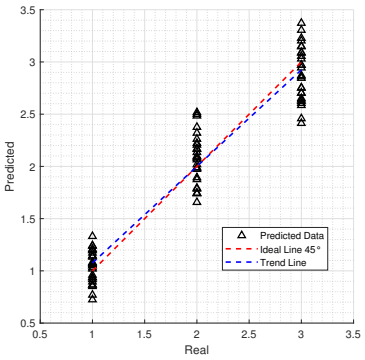
FFNN	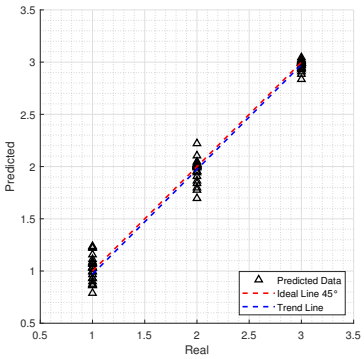	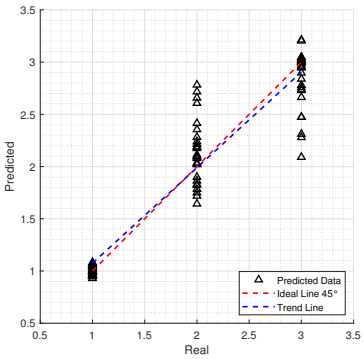	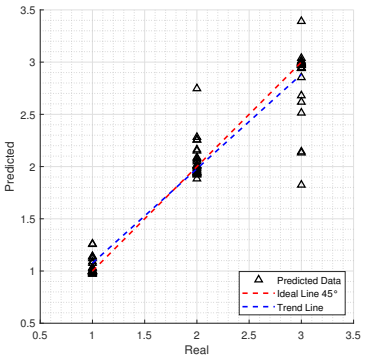

TABLE II. REAL VS. PREDICTED THICKNESS USING OPTIMIZED MODELS. SCATTER PLOTS FOR SVR, BRT, PLSR, AND FFNN AFTER MODEL OPTIMIZATION, APPLIED TO PS, EPM, AND MS FILMS. THE 45° LINE SHOWS IDEAL PREDICTIONS; TREND LINES INDICATE MODEL PERFORMANCE IMPROVEMENTS

Models	PS	EPM	MS
SVR	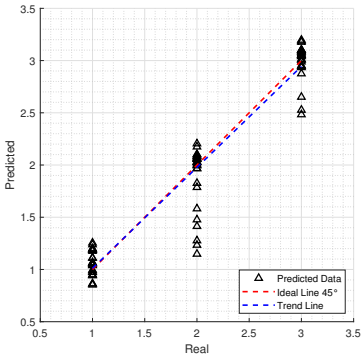	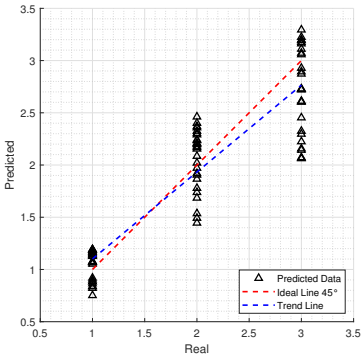	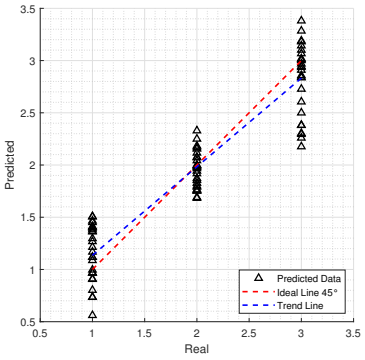
BRT	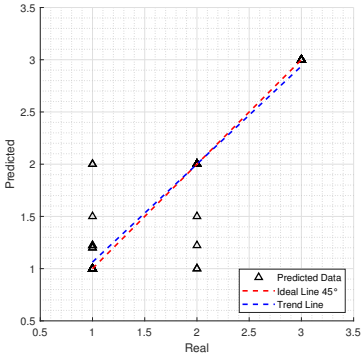	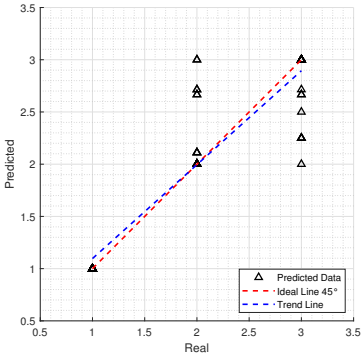	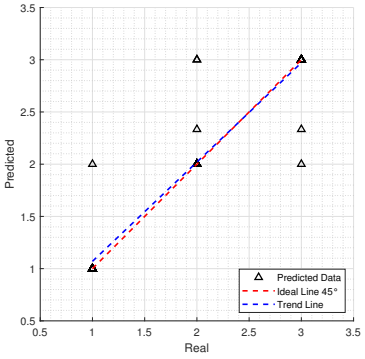
PLSR	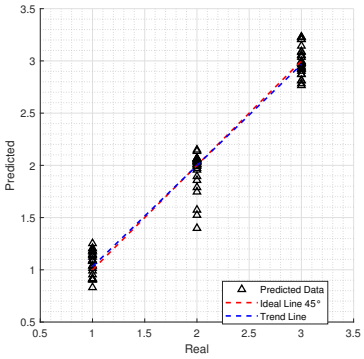	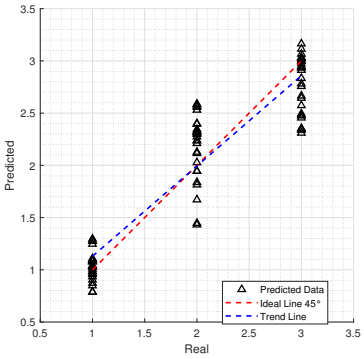	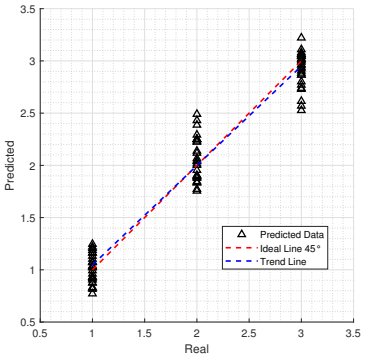
FFNN	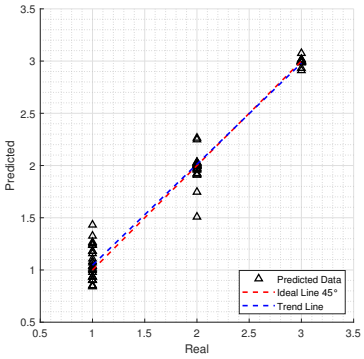	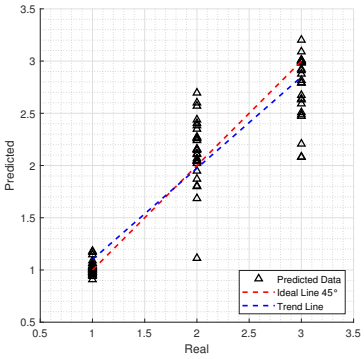	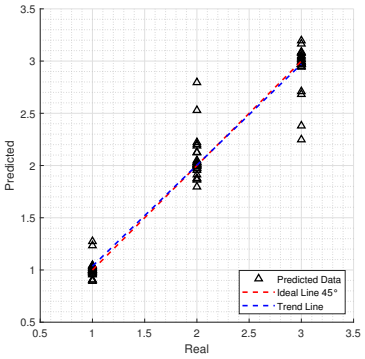

TABLE III. PERFORMANCE METRICS OF REGRESSION MODELS FOR THICKNESS PREDICTION. COEFFICIENT OF DETERMINATION, ROOT MEAN SQUARE ERROR, AND RATIO OF PERFORMANCE TO DEVIATION FOR PLSR, SVR, BRT, AND FFNN MODELS (FULL AND OPTIMIZED) ACROSS PS, EPM, AND MS SAMPLES. VALUES ARE PRESENTED AS MEAN ± STANDARD DEVIATION

Starch	Model	Type	R^2	RMSE	RPD
PS	PLSR	Full	0.9490 ± 0.0460	0.1843 ± 0.0028	4.4301 ± 0.3271
		Optimized	0.9645 ± 0.0117	0.1537 ± 0.0316	5.3129 ± 0.0412
	SVR	Full	0.9350 ± 0.0030	0.2097 ± 0.0049	3.9205 ± 0.0907
		Optimized	0.9237 ± 0.0030	0.2291 ± 0.0044	3.5881 ± 0.0687
	BRT	Full	0.8606 ± 0.0198	0.3100 ± 0.0219	2.6629 ± 0.1901
		Optimized	0.9303 ± 0.0247	0.2173 ± 0.0349	3.8552 ± 0.4904
	FFNN	Full	0.9757 ± 0.0104	0.1259 ± 0.0263	6.8106 ± 1.4711
		Optimized	0.9625 ± 0.0157	0.1573 ± 0.0335	5.4438 ± 1.1147
EPM	PLSR	Full	0.8599 ± 0.0210	0.3058 ± 0.0386	2.6704 ± 0.0249
		Optimized	0.8594 ± 0.0952	0.3063 ± 0.0611	2.6660 ± 0.1652
	SVR	Full	0.8425 ± 0.0046	0.3278 ± 0.0048	2.5066 ± 0.0366
		Optimized	0.8379 ± 0.0040	0.3368 ± 0.0037	2.4399 ± 0.0267
	BRT	Full	0.8425 ± 0.0046	0.3278 ± 0.0048	2.5066 ± 0.0366
		Optimized	0.8771 ± 0.0207	0.2874 ± 0.0246	2.8781 ± 0.2384
	FFNN	Full	0.8631 ± 0.0314	0.3032 ± 0.0361	2.7474 ± 0.3263
		Optimized	0.8712 ± 0.0172	0.2946 ± 0.0204	2.8015 ± 0.1849
MS	PLSR	Full	0.9171 ± 0.0635	0.2351 ± 0.0039	3.4723 ± 0.0583
		Optimized	0.9504 ± 0.0048	0.1819 ± 0.0141	4.4899 ± 0.1326
	SVR	Full	0.8915 ± 0.0056	0.2701 ± 0.0074	3.0439 ± 0.0827
		Optimized	0.8623 ± 0.0028	0.3038 ± 0.0029	2.7044 ± 0.0260
	BRT	Full	0.9002 ± 0.0154	0.2602 ± 0.0201	3.1751 ± 0.2395
		Optimized	0.9211 ± 0.0119	0.2306 ± 0.0174	3.5817 ± 0.2695
	FFNN	Full	0.9305 ± 0.0216	0.2154 ± 0.0333	3.8984 ± 0.5758
		Optimized	0.9422 ± 0.0113	0.1964 ± 0.0192	4.2218 ± 0.4152

All four models demonstrated solid outcomes, aligning with the limited research on polymer analysis via THz spectroscopy and regression modeling. In particular, [40] evaluated polyethylene mixed with carbendazim, obtaining strong results for SVR (R = 0.9972, RMSEP = 0.02) and PLSR (R = 0.9957, RMSEP = 0.0255). Likewise, [41] predicted antioxidant content in low-density polyethylene films through PLSR ($R^2 = 0.999$), and [42] investigated 2-mercaptobenzimidazole (MB) content in mixtures of MB, zinc oxide, silica, N, N'-Diphenyl-p-phenylenediamine, and nitrile-butadiene using PLSR (R = 0.9269, RMSEC = 2.9108) and SVR (R = 0.9760, RMSEC = 1.6899). No recent research has adopted FFNN or BRT with THz-TDS for polymer analysis. BRT has been used for other sample types with promising results, and FFNN may represent the first instance of combining this model with THz-TDS for polymer analysis.

C. Summary of Results

In summary, the spectral analysis confirms that the thickness of the film substantially influences the characteristics of the THz signal in both the time and the frequency domain. Furthermore, the regression models, particularly PLSR and FFNN, demonstrated strong predictive capabilities, thereby validating the feasibility of using THz-TDS in conjunction with advanced machine learning techniques for the non-invasive determination of bioplastic film thickness.

D. Limitations

This research presents certain limitations that should be considered in future studies. Among these, the following stand out:

- *Sample composition variability:* Variability in sample composition may have influenced spectral response, particularly since factors such as plasticizer type or residual moisture content were not evaluated.
- *THz spectral range:* Only the 0.5 to 1.2 THz range was analyzed, selected due to its sensitivity to thickness changes. Noise levels at frequencies above 1.4 THz limited the full utilization of the available spectral range (0.1 to 10 THz).
- *Modeling approaches:* Although PLSR and FFNN demonstrated good performance, the SVR and BRT models exhibited higher variability, especially for EPM. This variability suggests that model selection should consider the specific type of samples being analyzed.
- *Device operation conditions:* Ambient humidity represents another limitation, as it negatively affects signals at high frequencies and can introduce additional variability in the measurements.
- *Sample shape uniformity:* While THz-TDS successfully identified patterns related to variations in thickness in starch-based bioplastics, its performance may be affected by factors such as sample homogeneity and surface roughness, highlighting the need for complementary analyzes to enhance sample characterization.

IV. Conclusion

This study evaluated the feasibility of integrating THz-TDS with advanced machine learning techniques for the non-invasive prediction of bioplastic film thickness. The experimental results demonstrated that variations in film thickness induce significant changes in both time- and frequency-domain spectral responses. Among the regression models applied, PLSR, SVR, and FFNN provided robust predictions with coefficients of determination exceeding 82%, while the BRT model exhibited greater prediction dispersion and compensation bias.

The findings confirm that the thickness of the film is a critical parameter that influences the mechanical and physical properties of bioplastic materials. The combined approach - using THz-TDS, chemometric analysis, and machine learning - offers a promising, non-invasive quality control method for producing sustainable packaging materials. Model optimization improved predictive performance, particularly for maize starch-based samples, emphasizing the importance of advanced feature selection and parameter tuning.

Future research should focus on refining feature extraction techniques and exploring additional machine learning models to improve predictive accuracy. The application of this integrated methodology may also be extended to other sustainable materials, broadening its impact on environmental preservation and advancing environmentally friendly technologies.

Acknowledgment

This project was funded by the *Programa Nacional de Investigación Científica y Estudios Avanzados* (PROCIENCIA) through the *Tesis de Pregrado y Posgrado en Ciencia, Tecnología e Innovación Tecnológica 2023* competition, under the project titled "*Evaluación del espesor y ratio de contenido de dos almidones en el perfil THz de biopelículas*", contract number PE501085439-2023-PROCIENCIA.

References

[1] A. Ancy, M. Lazar, A. S. Chandran, and M. Ushamani, "Development of ecofriendly and sustainable bioplastics from cassava starch: Tailoring the properties using nanoparticles," *Sustainable Chemistry and Pharmacy*, vol. 37, p. 101377, 2024, http://doi.org/10.1016/j.scp.2023.101377.

[2] M. Ghasemlou, F. Daver, B. J. Murdoch, A. S. Ball, E. P. Ivanova, and B. Adhikari, "Biodegradation of novel bioplastics made of starch, polyhydroxyurethanes and cellulose nanocrystals in soil environment," *Science of the Total Environment*, vol. 815, p. 152684, 2022, http://doi.org/10.1016/j.scitotenv.2021.152684.

[3] S. Islam, H. Jameel, and J. M. Cullen, "Multi-stage mfa for evaluating sustainable waste potential for bioplastics conversion in the circular economy: An examination of uk wastes to produce cellulose nanofibre," *Journal of Cleaner Production*, vol. 482, p. 144166, 2024, http://doi.org/10.1016/j.jclepro.2024.144166.

[4] M. Alonso-González, D. Castro-Criado, M. Felix, and A. Romero, "Evaluation of rice bran varieties and heat treatment for the development of protein/starch-based bioplastics via injection molding," *International Journal of Biological Macromolecules*, vol. 253, p. 127503, 2023, http://doi.org/10.1016/j.ijbiomac.2023.127503.

[5] K. Synani, K. Abeliotis, K. Velonia, A. Maragkaki, T. Manios, and K. Lasaridi, "Environmental impact and sustainability of bioplastic production from food waste," *Sustainability*, vol. 16, no. 13, p. 5529, 2024, http://doi.org/10.3390/su16135529.

[6] F. M. Lounis, F. Benhacine, and A. S. Hadj-Hamou, "Improving water barrier properties of starch based bioplastics by lignocellulosic biomass addition: Synthesis, characterization and antibacterial properties," *International Journal of Biological Macromolecules*, vol. 283, p. 137823, 2024, http://doi.org/10.1016/j.ijbiomac.2024.137823.

[7] S. Xu, J. Cui, C. Dai, X. Wei, X. Tian, D. Fang, G. Song, and L. Ma, "From waste to eco-friendly biofilms: Harnessing cottonseed hull proanthocyanidins for sustainable solutions," *Environmental Technology & Innovation*, vol. 33, p. 103448, 2024, http://doi.org/10.1016/j.eti.2023.103448.

[8] M. M. Abe, M. C. Branciforti, R. N. Montagnolli, M. A. M. Morales, A. P. Jacobus, and M. Brienzo, "Production and assessment of the biodegradation and ecotoxicity of xylan-and starch-based bioplastics," *Chemosphere*, vol. 287, p. 132290, 2022, http://doi.org/10.1016/j.chemosphere.2021.132290.

[9] S. González-Rojo, A. Paniagua-García, and R. Díez-Antolínez, "Biotransformation of starch-based wastewater into bioplastics: Optimization of poly (3-hydroxybutyrate) production by cupriavidus necator dsm 545 using potato wastewater hydrolysate," *Water Research*, vol. 247, p. 120766, 2023, http://doi.org/10.1016/j.watres.2023.120766.

[10] M. Alonso-González, M. Felix, A. Guerrero, and A. Romero, "Rice bran-based bioplastics: Effects of the mixing temperature on starch plastification and final properties," *International Journal of Biological Macromolecules*, vol. 188, pp. 932–940, 2021, http://doi.org/10.1016/j.ijbiomac.2021.08.043.

[11] C. M. Granados-Carrera, D. Castro-Criado, M. Jiménez-Rosado, A. Romero, and V. M. Perez-Puyana, "Reinforcement of soy protein-based bioplastics as potential sustainable packaging solutions," *Future Foods*, vol. 11, p. 100524, 2025, http://doi.org/10.1016/j.fufo.2024.100524.

[12] S. Diah, S. Abdullah, Y. Seok, I. Fatah, N. I. A. Rahman, F. Hafizulhaq, and N. Alias, "Towards sustainable food packaging: A review of thermoplastic starch (TPS) as a promising bioplastic material, its limitations, and improvement strategies with bio-fillers and essential oils," *J. Adv. Res. Fluid Mech. Therm. Sci*, vol. 119, pp. 80–104, 2024, http://doi.org/10.37934/arfmts.119.1.80104.

[13] M. L. Rojas, D. Asmat-Campos, A. Carreño-Ortega, and N. Raquel-Checca, "Physical and thermal improvement of bioplastics based on potato starch/agar composite functionalized with biogenic zno nanoparticles," *International Journal of Biological Macromolecules*, vol. 282, p. 137468, 2024, http://doi.org/10.1016/j.ijbiomac.2024.137468.

[14] J. Yang, S. Xu, Y. C. Ching, C. H. Chuah, R. Wang, C. Li, Y. Wei, and G. Liang, "Effects of silane hydrolysis time on the physicochemical properties of bioplastics based on starch and epoxidized soybean oil," *Food Chemistry*, vol. 460, p. 140601, 2024, http://doi.org/10.1016/j.foodchem.2024.140601.

[15] V. Grossule, S. Zanatta, M. Modesti, and M. C. Lavagnolo, "Treatment of food waste contaminated by bioplastics using BSF larvae: Impact and fate of starch-based bioplastic films," *Journal of environmental management*, vol. 330, p. 117229, 2023, http://doi.org/10.1016/j.jenvman.2023.117229.

[16] H. Guo, P. Prempree, S. Chen, Y. Yamashige, N. Kondo, and Y. Ogawa, "Crystallinity determination of amylose-fatty acid complex in gelatinized rice starch-fatty acid mixtures using terahertz spectroscopy," *Food Hydrocolloids*, vol. 146, p. 109279, 2024, http://doi.org/10.1016/j.foodhyd.2023.109279.

[17] I. Oliver, N. Martínez-Pérez, A. Fullana, and J. A. Conesa, "Impact of bioplastic design on biodigestion treatment," *Sustainability*, vol. 16, no. 16, p. 7167, 2024, http://doi.org/10.3390/su16167167.

[18] N. Vijayakumar, A. V. Sanjay, K. A. Al-Ghanim, M. Nicoletti, G. Baskar, R. Kumar, and M. Govindarajan, "Development of biodegradable bioplastics with sericin and gelatin from silk cocoons and fish waste," *Toxics*, vol. 12, no. 7, p. 453, 2024, http://doi.org/10.3390/toxics12070453.

[19] R. Ratna, M. Mutia, D. Darwin, A. A. Munawar, F. Fitriani, and L. Handayani, "Utilization of tofu liquid waste for the manufacture of bioplastic food packaging," *Case Studies in Chemical and Environmental Engineering*, vol. 10, p. 100830, 2024, http://doi.org/10.2139/ssrn.4818775.

[20] O. Oluwasina, A. Aderibigbe, S. Ikupoluyi, O. Oluwasina, and T. Ewetumo, "Physico-electrical properties of starch-based bioplastic enhanced with acid-treated cellulose and graphene oxide fillers," *Sustainable Chemistry for the Environment*, vol. 6, p. 100093, 2024, http://doi.org/10.1016/j.scenv.2024.100093.

[21] O. Oluwasina, M. Adebayo, M. Akinsola, T. Olorunfemi, and J. Olajide, "Influence of 2-hydroxyethyl terephthalate from waste polyethylene plastic on the properties of starch-BHET bioplastics," *Waste Management Bulletin*, vol. 2, no. 1, pp. 203–213, 2024, http://doi.org/10.1016/j.wmb.2024.01.008.

[22] T. Read, C. M. Chan, C. Chaléat, B. Laycock, S. Pratt, and P. Lant, "The effect of additives on the biodegradation of polyhydroxyalkanoate (PHA) in marine field trials," *Science of The Total Environment*, vol. 931, p. 172771, 2024, http://doi.org/10.2139/ssrn.4681392.

[23] S. Azmin, I. Nasrudin, M. Nor, P. Abdullah, and H. Ch'Ng, "Development of food packaging bioplastic from potato peel starch incorporated with rice husk silica using response surface methodology comprehending central composite design," *Food Research*, 2024, http://doi.org/10.26656/fr.2017.8(s2).75.

[24] H. M. Aldawsari, S. Kotta, H. Z. Asfour, S. Vattamkandathil, M. A. Elfaky, L. Y. Ashri, and S. M. Badr-Eldin, "Development and evaluation of quercetin enriched bentonite-reinforced starch-gelatin based bioplastic with antimicrobial property," *Saudi Pharmaceutical Journal*, vol. 31, no. 12, p. 101861, 2023, http://doi.org/10.1016/j.jsps.2023.101861.

[25] N. V. Penkov, M. V. Goltyaev, M. E. Astashev, D. A. Serov, M. N. Moskovskiy, D. O. Khort, and S. V. Gudkov, "The application of terahertz time-domain spectroscopy to identification of potato late blight and fusariosis," *Pathogens*, vol. 10, no. 10, p. 1336, 2021, http://doi.org/10.3390/pathogens10101336.

[26] M. Zhao, F. Yan, W. Li, and Y. Liu, "Research on detection of food additives based on terahertz spectroscopy and analytic hierarchy process," *Instrumentation*, vol. 11, no. 1, pp. 30–37, 2024.

[27] H.-P. Wang, P. Chen, J.-W. Dai, D. Liu, J.-Y. Li, Y.-P. Xu, and X.-L. Chu, "Recent advances of chemometric calibration methods in modern spectroscopy: Algorithms, strategy, and related issues," *TrAC Trends in Analytical Chemistry*, vol. 153, p. 116648, 2022, http://doi.org/10.1016/j.trac.2022.116648.

[28] R. Jimenez, G. Sandoval-Flores, S. Alvarado-Reyna, S. E. Aleman-Castillo, R. Santiago-Adame, and G. Velazquez, "Extraction of starch from hass avocado seeds for the preparation of biofilms," *Food Science and Technology*, vol. 42, p. e56820, 2021, http://doi.org/10.1590/fst.56820.

[29] A. Sultan, H. Sultan, W. Shahzad, A. Kareem, A. Liaqat, Z. Ashraf, A. Shahid, A. Rauf, S. Saeed, T. Mehmood *et al.*, "Comparative analysis of physical and mechanical properties of starch based bioplastic derived from the pulp and peel of potatoes," *Journal of the Indian Chemical Society*, vol. 101, no. 10, p. 101301, 2024, http://doi.org/10.1016/j.jics.2024.101301.

[30] M. Alonso-González, M. Felix, and A. Romero, "Development of rice bran-based bioplastics via injection molding: Influence of particle size and glycerol ratio," *Resources, Conservation and Recycling*, vol. 208, p. 107713, 2024, http://doi.org/10.1016/j.resconrec.2024.107713.

[31] F. Kahvand and M. Fasihi, "Plasticizing and anti-plasticizing effects of polyvinyl alcohol in blend with thermoplastic starch," *International journal of biological macromolecules*, vol. 140, pp. 775–781, 2019, http://doi.org/10.1016/j.ijbiomac.2019.08.185.

[32] C. R. Contessa, N. B. de Souza, G. B. Gonçalo, C. M. de Moura, G. S. da Rosa, and C. C. Moraes, "Development of active packaging based on agar-agar incorporated with bacteriocin of *Lactobacillus sakei*," *Biomolecules*, vol. 11, no. 12, p. 1869, 2021, http://doi.org/10.3390/biom11121869.

[33] M. Marichelvam, M. Jawaid, and M. Asim, "Corn and rice starch-based bio-plastics as alternative packaging materials," *Fibers*, vol. 7, no. 4, p. 32, 2019, http://doi.org/10.3390/fib7040032.

[34] R. Rosipal and N. Krämer, "Overview and recent advances in partial least squares," in *International Statistical and Optimization Perspectives Workshop" Subspace, Latent Structure and Feature Selection"*. Springer, 2005, pp. 34–51, http://doi.org/10.1007/11752790_2.

[35] S. Riaz, N. Ahmad, W. Farooq, I. Ali, M. Sajid, and M. N. Akhtar, "Catalytic pyrolysis of hdpe for enhanced hydrocarbon yield: A boosted regression tree assisted kinetics study for effective recycling of waste plastic," *Digital Chemical Engineering*, vol. 14, p. 100213, 2025, http://doi.org/10.1016/j.dche.2024.100213.

[36] N. A. Almansour, H. F. Syed, N. R. Khayat, R. K. Altheeb, R. E. Juri, J. Alhiyafi, S. Alrashed, and S. O. Olatunji, "Neural network and support vector machine for the prediction of chronic kidney disease: A comparative study," *Computers in biology and medicine*, vol. 109, pp. 101–111, 2019, http://doi.org/10.1016/j.compbiomed.2019.04.017.

[37] M. M. Jibril, M. Zayyan, S. I. Malami, A. Usman, B. A. Salami, A. Rotimi, and S. Abba, "Implementation of nonlinear computing models and classical regression for predicting compressive strength of high-performance concrete," *Applications in Engineering Science*, vol. 15, no. N/A, p. 100133, 2023, https://doi.org/10.1016/j.apples.2023.100133.

[38] N. Vásquez, C. Magán, J. Oblitas, T. Chuquizuta, H. Avila-George, and W. Castro, "Comparison between artificial neural network and partial least squares regression models for hardness modeling during the ripening process of swiss-type cheese using spectral profiles," *Journal of Food Engineering*, vol. 219, pp. 8–15, 2018, https://doi.org/10.1016/j.jfoodeng.2017.09.008.

[39] V. Tirado-Kulieva, C. Quijano-Jara, H. Avila-George, and W. Castro, "Predicting the evolution of ph and total soluble solids during coffee fermentation using near-infrared spectroscopy coupled with chemometrics," *Current Research in Food Science*, vol. 9, p. 100788, 2024, https://doi.org/10.1016/j.crfs.2024.100788.

[40] B. Qin, Z. Li, Z. Luo, H. Zhang, and Y. Li, "Feasibility of terahertz time-domain spectroscopy to detect carbendazim mixtures wrapped in paper," *Journal of Spectroscopy*, vol. 2017, no. 1, p. 6302868, 2017, http://doi.org/10.1155/2017/6302868.

[41] T. Ogishima, C. Kuroda, N. Hirai, and Y. Ohki, "Broadband fir absorption spectra of low-density polyethylene sheets containing six different antioxidants and estimation of their contents by chemometric analysis," *High Voltage*, vol. 4, no. 3, pp. 161–166, 2019, http://doi.org/10.1049/hve.2019.0074.

[42] X. Yin, H. Chen, and H. Zhang, "Quantitative detection of multi-component rubber additives based on terahertz spectral data fusion," *High Voltage*, vol. 51, no. 5, 2024, http://doi.org/10.3788/CJL230807.